Microseismic forward modeling based on different focal mechanisms used by the seismic moment tensor and elastic wave equation

2015 J. Geophys. Eng. 12 155

(http://iopscience.iop.org/1742-2140/12/2/155)

IOP Publishing Journal of Geophysics and Engineering
J. Geophys. Eng. **12** (2015) 155–166 doi:10.1088/1742-2132/12/2/155

Microseismic forward modeling based on different focal mechanisms used by the seismic moment tensor and elastic wave equation

Huijian Li, Runqiu Wang and Siyuan Cao

State Key Laboratory of Petroleum Resources and Prospecting, CNPC Key Laboratory of Geophysical Exploration, China University of Petroleum, Beijing, People's Republic of China

E-mail: lihuijian1117@163.com

Received 9 August 2014, revised 8 December 2014
Accepted for publication 12 December 2014
Published 4 February 2015

Abstract

The source mechanisms of microseismics in hydraulic fracturing present guiding significance to the research on source types, crustal stress analysis and crack prediction. Numerical simulations based on various source mechanisms can be used to investigate the stress characteristics and response characteristics of different source types. In this paper, a method based on the seismic moment tensor (SMT) and elastic wave equation (EWE) was presented for forward modeling. Additionally, we have given the expressions of nine couples of force which can be combined into different kinds of source types. The calculations of wave fields and records with three basic types of sources showed the features in homogeneous isotropic and anisotropic media by the finite-difference (FD) method. Lastly, analysis of the relationship between the polarizing angle and incident angle provided us with some evidence to distinguish the type of media in single media. The work offers methods of instruction for identification and interpretation in microseismic monitoring.

Keywords: microseismic forward modeling, seismic moment tensor, elastic wave equation, focal mechanism, finite-difference, polarization

(Some figures may appear in colour only in the online journal)

1. Introduction

Microseismic monitoring is an effective way to observe the effect of hydraulic fracturing (Maxwell 2010). It is complex and difficult to predict the fracturing system. The signals generated by different kinds of sources are also distinguishing. The microseismic moment tensor (SMT) has great potential toward realizing the process of fracturing and microseismic events, since it can reveal important information about the fracturing process (Baig and Urbancic 2010). The simulation of SMTs can display the features of waveform and wave field, which will be helpful for further understanding and full use of three-component data.

Any source mechanism can be mathematically decomposed into three components: isotropic (ISO), double couple (DC), and compensated linear vector dipole (CLVD) (Knopoff and Randall 1970). The pure ISO source is associated with explosive or implosive force; the pure DC source is caused by shear faulting which is familiar in hydrofracture; and the CLVD source is accompanied by the ISO source but is more complicated (Vavryčuk 2001).

Seismic forward modeling can mainly be implemented by two strategies: analytical expression and numerical solution (e.g. finite-element method, finite-difference (FD) method and pseudo-spectral method). The former yields the records of various sources in simple media (such as homogeneous media) by Green function method (Li *et al* 1990) and has a fast calculation speed. However, it requires the exact velocity formulae for media. Moreover, it is difficult to be employed in complex media. Therefore, the explicit analytical formulae for the acoustic and elastodynamic 3D

Green functions were proposed (Holfold 1981, Jeng and Liu 1987, Li *et al* 1990). Nevertheless, they were not an explicit closed-form solution for the media (Vavryčuk 2000). The method is extensively used in seismic exploration (e.g. Yuan *et al* 2014) and is mainly utilized to study the characteristics of wave field and records with various complex media (e.g. Coutant *et al* 1995). Owing to easy implementation and high efficiency, the FD method (e.g. Bansal and Sen 2008) is the most commonly used. Although the computation speed is lower than the analytical method, the advantage is that it can fit complex media.

Sources in seismic forward modeling based on elastic wave equations (EWEs) are normally explosive ones. But the sources caused by hydrofracture are intricate which not only include the explosive source but also contain DC sources and CLVD sources (Baig and Urbancic 2010). Therefore, the issue of how to simulate various sources becomes an important part of wave field stimulation in microseismic monitoring. In this paper, we combine SMT as source mechanism expressions in earthquake seismology with EWE. We also present the expressions of three basic sources for the FD method. Subsequently, wave field and records in different media are gained. Their characteristics could provide the evidence for fast interpretation in microseismic data processing. Compared with focal mechanism forward modeling based on Green's function, the waveforms and records are more realistic.

2. Theory

2.1. Elastic wave equation

The 3D EWE in homogeneous anisotropic media can be written as (Tsvankin 2012)

$$\rho\frac{\partial^2 u_i}{\partial t^2} - C_{ijkl}\frac{\partial^2 u_k}{\partial x_j \partial x_l} = f_i, \qquad i,j,k,l = 1,2,3, \tag{1}$$

where u_i and u_k are the displacement fields, C_{ijkl} is the stiffness tensor, ρ is the density, f_i is the body force, and t is the propagation time. In general, the body force f_i added in conventional seismic forward modeling ignores the angle information. In fact, microseismic events caused by fracturing include the strike angle, dipping direction angle and dipping angle of fractures. What is more, the SMT is a path to understand the source and crack growth (Baig and Urbancic 2010). Thus, we used a combination of moment tensors with EWEs to illustrate the basic sources: ISO, DC and CLVD. Distributions of body forces that are added to the individual components of velocity in a staggered-grid system were employed. This approach follows the method proposed by Graves (1996), with appropriate modifications on the strength and form of moment-tensor components. The modified formulae adapted to staggered mesh and variable mesh algorithms.

2.2. Source excitation method

There are mainly two kinds of source excitation methods in the staggered-grid FD algorithm: adding to the stress components (Coutant *et al* 1995, Olsen *et al* 1995) and adding to the velocity components (Yomogida and Etgen 1993, Graves 1996). Here, we present a source excitation method which added body forces to the individual components of velocity. Our approach is similar to the method of Graves (1996), which added a source on velocity component, and the approach proposed by Coutant *et al* (1995) which used the stress component. The difference is that we modify the expression and the form of SMT components.

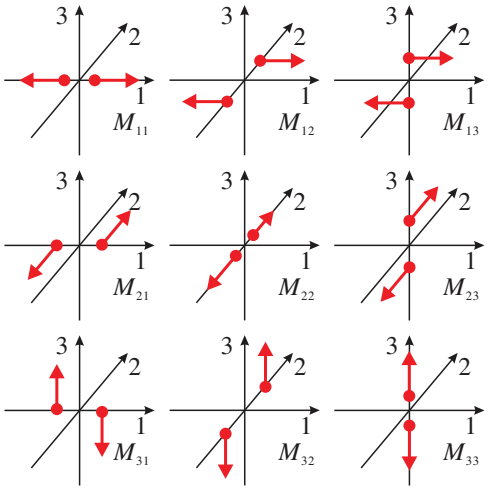

Figure 1. SMTs with nine possible couples.

All kinds of sources can be illustrated by the combinations of the nine force couples (Aki and Richards 2002) (figure 1), which can be expressed as:

$$\mathbf{M} = \begin{bmatrix} M_{11} & M_{12} & M_{13} \\ M_{21} & M_{22} & M_{23} \\ M_{31} & M_{32} & M_{33} \end{bmatrix}, \tag{2}$$

where $\mathbf{M}$ is the moment tensor, M_{ij} (i = 1, 2, 3; j = 1, 2, 3) is each element of force. We first discuss the moment tensor contributions to the x component of the body forces fx. It includes three components: M_{11}, M_{12} and M_{13}, which represent the acting points at x, y and z coordinate respectively (figure 1). The moment tensor has a moment arm of length dx. The equivalent body force distribution of M_{11} is given by

$$fx_{i+1/2,j,k} = \frac{M_{11}\cdot \mathrm{d}t}{\rho\cdot V\cdot \mathrm{d}x}\cdot f(t)\,, fx_{i-1/2,j,k} = -\frac{M_{11}\cdot \mathrm{d}t}{\rho\cdot V\cdot \mathrm{d}x}\cdot f(t)\,, \tag{3}$$

where dt is the sampling interval, $V = \mathrm{d}x\cdot\mathrm{d}y\cdot\mathrm{d}z$ is the volume of the grid cell, and $f(t)$ is the dimensionless-wavelet with normalization. Similarly, the equivalent body-force distributions for M_{12} and M_{13} are given by

$$fx_{i+1/2,j,k} = \frac{M_{12}\cdot \mathrm{d}t}{\rho\cdot V\cdot \mathrm{d}y}\cdot f(t)\,, fx_{i+1/2,j-1,k} = -\frac{M_{12}\cdot \mathrm{d}t}{\rho\cdot V\cdot \mathrm{d}y}\cdot f(t)\,, \tag{4}$$

and

$$fx_{i+1/2,j,k} = \frac{M_{13}\cdot \mathrm{d}t}{\rho\cdot V\cdot \mathrm{d}z}\cdot f(t)\,, fx_{i+1/2,j,k-1} = -\frac{M_{13}\cdot \mathrm{d}t}{\rho\cdot V\cdot \mathrm{d}z}\cdot f(t)\,. \tag{5}$$

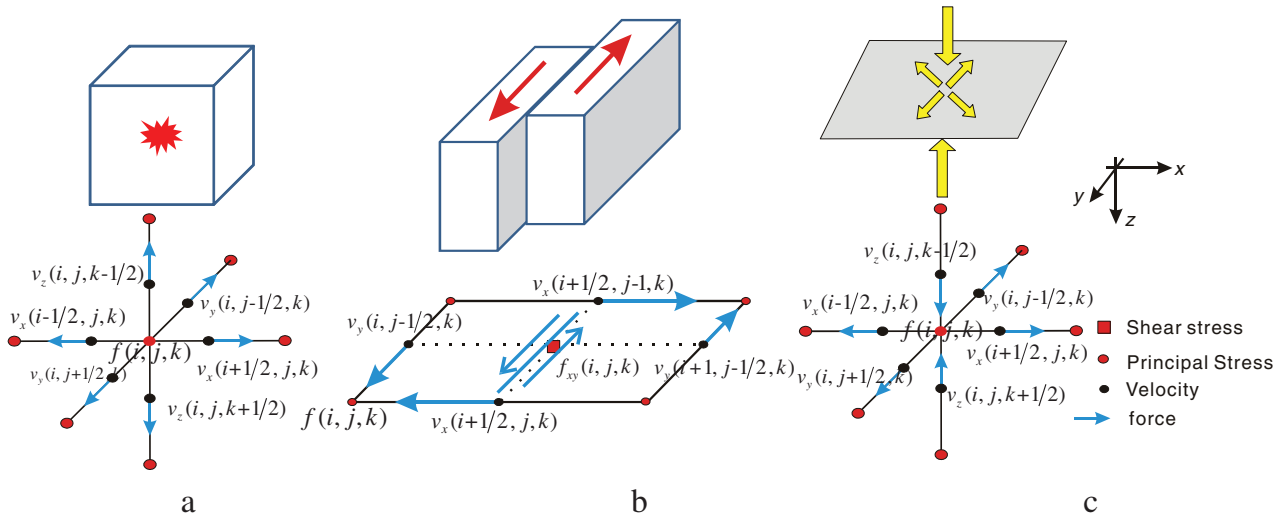

Figure 2. Sketch map and FD schemes of three kinds of sources. (*a*) ISO source as explosive source an example. (*b*) DC source of shear force on the *x*–*y* plane. (*c*) CLVD source. Red circles represent principal stress, red boxes are shear stress, black circles are velocities and blue arrows represent the directions of force.

The formulae for the distribution of body forces *fy* and *fz*, can be derived in a similar fashion. These expressions are given in the appendix.

The body forces in the other two components *fy* and *fz* have similar equations. Using these nine couples of force, all the ISO, DC and CLVD sources can be generated. Here, only three basic representative sources are taken into account. Their moment tensors are (Vavryčuk 2005)

$$\mathrm{M_{ISO}} = \begin{bmatrix} M_{11} & 0 & 0 \\ 0 & M_{22} & 0 \\ 0 & 0 & M_{33} \end{bmatrix}, \mathrm{M_{DC}} = \begin{bmatrix} 0 & M_{12} & 0 \\ M_{21} & 0 & 0 \\ 0 & 0 & 0 \end{bmatrix}, \quad \mathrm{M_{CLVD}} = \begin{bmatrix} M_{11} & 0 & 0 \\ 0 & M_{22} & 0 \\ 0 & 0 & -2M_{33} \end{bmatrix}. \tag{6}$$

Figure 2 shows the sketch map of three basic sources and their FD schemes. We consider the ISO component as an explosive source, with three couples of body forces in three components. The middle point (figure 2(*a*) circle point) is principal stress, whereas black points are velocity. In the staggered-grid FD method, the principal stress $f(i,j,k)$ is calculated by six points of velocity. So we add three couples of force (arrows in blue) as the initial conditions. The DC component is different from the ISO, which represents a transform fault in horizontal plane in this paper (figure 2(*b*)). The fault is mainly caused by shear stress f_{xy} (figure 2(*b*) square point), calculated by two couples of body forces on *Vx* and *Vy*. That is, SMTs M_{12} and M_{21} can generate the stress force. CLVD component usually couples with the ISO component. As figure 2(*c*) shows, there are also three couples of force. But the force in one side is opposite to the other sides. In other words, one couple of force is compressive stress and others are tensile stress. ISO source and CLVD source belong to non-DC components in earthquake seismology. The detailed expressions of these three sources are:

$$\begin{aligned}
\Delta V_x^{n+1/2}(i+1/2,j,k) &= \frac{M_{11}\cdot \mathrm{d}t}{\rho\cdot V\cdot \mathrm{d}x}\cdot f(\mathrm{d}t\cdot n) \\
\Delta V_x^{n+1/2}(i-1/2,j,k) &= -\frac{M_{11}\cdot \mathrm{d}t}{\rho\cdot V\cdot \mathrm{d}x}\cdot f(\mathrm{d}t\cdot n) \\
\Delta V_y^{n+1/2}(i,j+1/2,k) &= \frac{M_{22}\cdot \mathrm{d}t}{\rho\cdot V\cdot \mathrm{d}y}\cdot f(\mathrm{d}t\cdot n) \\
\Delta V_y^{n+1/2}(i,j-1/2,k) &= -\frac{M_{22}\cdot \mathrm{d}t}{\rho\cdot V\cdot \mathrm{d}y}\cdot f(\mathrm{d}t\cdot n), \\
\Delta V_z^{n+1/2}(i,j,k+1/2) &= \frac{M_{33}\cdot \mathrm{d}t}{\rho\cdot V\cdot \mathrm{d}z}\cdot f(\mathrm{d}t\cdot n) \\
\Delta V_z^{n+1/2}(i,j,k-1/2) &= -\frac{M_{33}\cdot \mathrm{d}t}{\rho\cdot V\cdot \mathrm{d}z}\cdot f(\mathrm{d}t\cdot n)
\end{aligned} \tag{7}$$

$$\begin{aligned}
\Delta V_x^{n+1/2}(i+1/2,j,k) &= -\frac{M_{12}\cdot \mathrm{d}t}{\rho\cdot V\cdot \mathrm{d}x}\cdot f(\mathrm{d}t\cdot n) \\
\Delta V_x^{n+1/2}(i+1/2,j-1,k) &= \frac{M_{12}\cdot \mathrm{d}t}{\rho\cdot V\cdot \mathrm{d}x}\cdot f(\mathrm{d}t\cdot n) \\
\Delta V_y^{n+1/2}(i,j-1/2,k) &= \frac{M_{21}\cdot \mathrm{d}t}{\rho\cdot V\cdot \mathrm{d}y}\cdot f(\mathrm{d}t\cdot n), \\
\Delta V_y^{n+1/2}(i+1,j-1/2,k) &= -\frac{M_{21}\cdot \mathrm{d}t}{\rho\cdot V\cdot \mathrm{d}y}\cdot f(\mathrm{d}t\cdot n)
\end{aligned} \tag{8}$$

$$\begin{aligned}
\Delta V_x^{n+1/2}(i+1/2,j,k) &= \frac{M_{11}\cdot \mathrm{d}t}{\rho\cdot V\cdot \mathrm{d}x}\cdot f(\mathrm{d}t\cdot n) \\
\Delta V_x^{n+1/2}(i-1/2,j,k) &= -\frac{M_{11}\cdot \mathrm{d}t}{\rho\cdot V\cdot \mathrm{d}x}\cdot f(\mathrm{d}t\cdot n) \\
\Delta V_y^{n+1/2}(i,j+1/2,k) &= \frac{M_{22}\cdot \mathrm{d}t}{\rho\cdot V\cdot \mathrm{d}y}\cdot f(\mathrm{d}t\cdot n), \\
\Delta V_y^{n+1/2}(i,j-1/2,k) &= -\frac{M_{22}\cdot \mathrm{d}t}{\rho\cdot V\cdot \mathrm{d}y}\cdot f(\mathrm{d}t\cdot n) \\
\Delta V_z^{n+1/2}(i,j,k+1/2) &= -2\cdot\frac{M_{33}\cdot \mathrm{d}t}{\rho\cdot V\cdot \mathrm{d}z}\cdot f(\mathrm{d}t\cdot n) \\
\Delta V_z^{n+1/2}(i,j,k-1/2) &= 2\cdot\frac{M_{33}\cdot \mathrm{d}t}{\rho\cdot V\cdot \mathrm{d}z}\cdot f(\mathrm{d}t\cdot n)
\end{aligned} \tag{9}$$

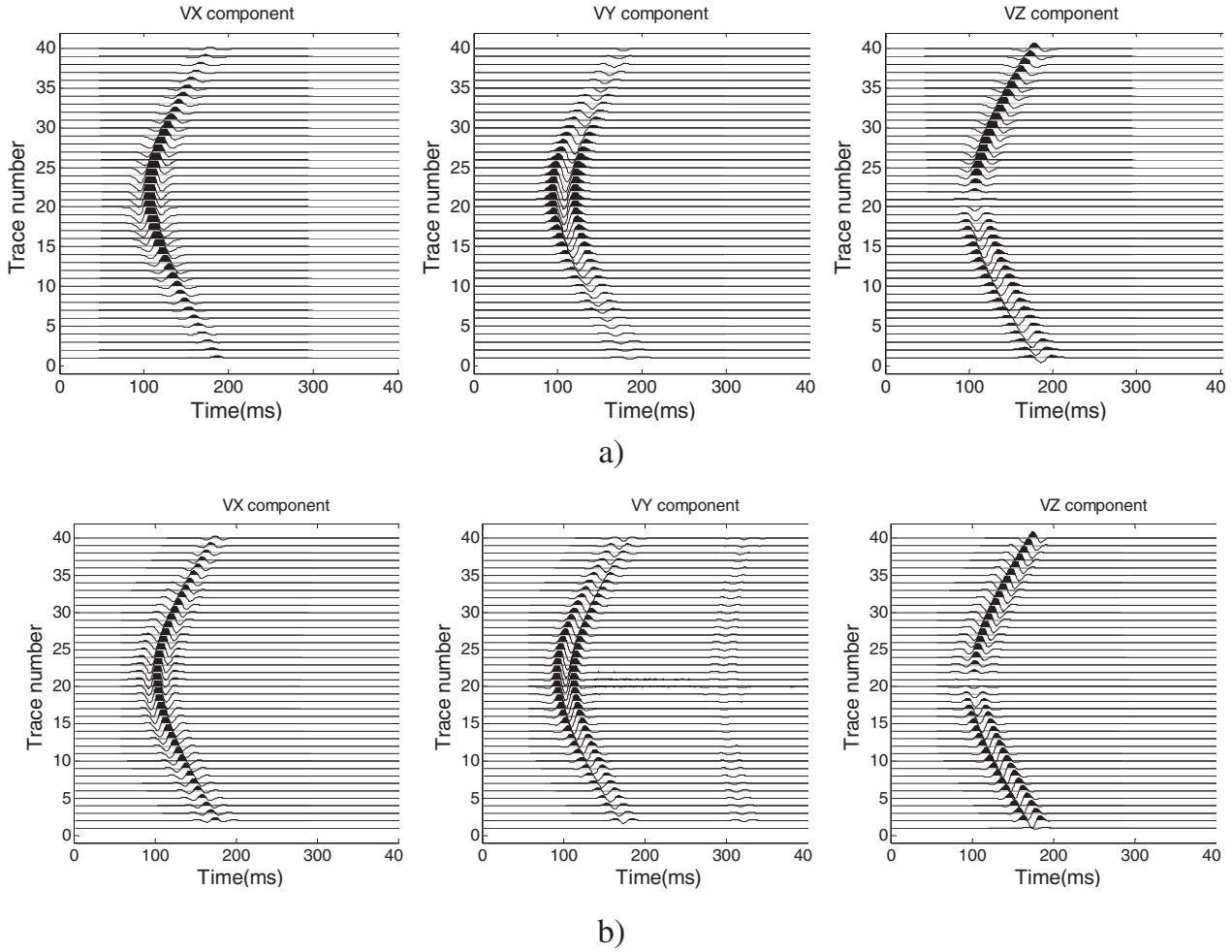

Figure 3. Green's function (*a*) compared with the new method (*b*) (SMT and EWE) in homogeneous isotropic media. (*a*) Records from *Vx*, *Vy* and *Vz* components based on Green's function; (*b*) from *Vx*, *Vy* and *Vz* components based on SMT and EWE method. The reference seismogram has been computed by using a small model to have boundary reflections arrive at about 300 ms in *Vy* component.

where $\Delta V_x^{n+1/2}(i+1/2, j, k)$ represents the velocity variation in *Vx* component on the point of $(i+1/2, j, k)$ at step $n+1/2$. $f(\mathrm{d}t \cdot n)$ is the wavelet at time of $\mathrm{d}t \cdot n$. When calculating the $(n+1/2)$th step of velocity field, the added force is equivalent to the variation of velocity. By using these three formulas, wave fields and records of three basic sources can be obtained. And the propagation under complex situation can be simulated by the combinational formulae.

The main idea is that source mechanisms can be described by SMT; we add it into EWE, which could fit in complex media; then, calculate the wave field and records by the FD method.

2.3. Comparison and verification

In earthquake seismology, Green's function is used for simulating DC and non-DC sources in simple media. Here, we apply a homogeneous isotropic model to verify the effectiveness of the method mentioned above (SMT and EWE). Besides, the comparison between it and Green's function is performed.

Figure 3(*a*) shows the records from *Vx*, *Vy* and *Vz* components with ISO source by Green's function, while figure 3(*b*) is based on SMT and EWE method. P-wave only can be recorded. Phase reversal appears in the *Vz* component. The result of the SMT and EWE method shown in figure 3(*b*) is nearly the same as figure 3(*a*). It can be realized that their

Table 1. The parameters of three kinds of sources and their beachballs.

Source types	Dip (°)	Slip (°)	Strike (°)	Receivers location in horizontal plane (m)	Beachball
ISO	0	0	0	(600,400)	
DC	45	0	45	(600,400)	
CLVD	90	−90	0	(600,400)	

Table 2. stiffness coefficients of four kinds of media (units: MPa).

Media	C_{11}	C_{22}	C_{33}	C_{44}	C_{55}	C_{66}	C_{12}	C_{13}	C_{23}
Homogeneous	22.53	22.53	22.53	7.13	7.13	7.13	8.27	8.27	8.27
VTI	26.39	26.39	15.6	4.38	4.38	6.84	12.71	6.11	6.11
HTI	21	23.5	23.5	7.13	4.41	4.41	8.5	8.5	9.24
Orthotropic	25.66	23.69	19.74	7.86	6.38	9.44	8.02	9.35	7.91

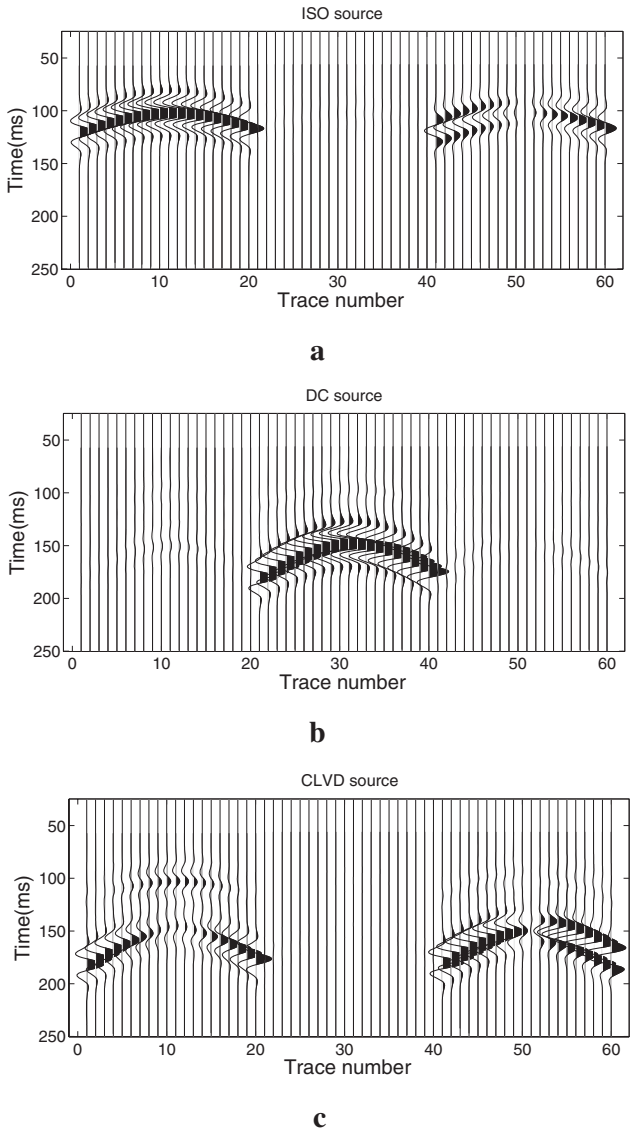

Figure 4. 3D three-component records of ISO, DC and CLVD sources in homogeneous media. (*a*) Records of *Vx* component; (*b*) records of *Vy* component; (*c*) records of *Vz* component.

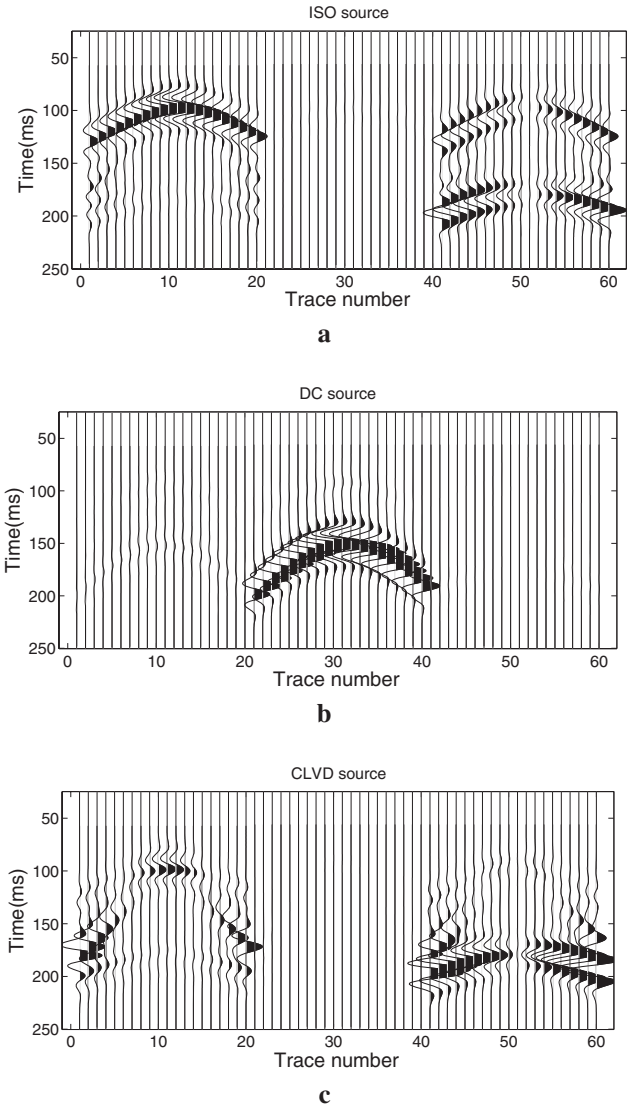

Figure 5. 3D three-component records of ISO, DC and CLVD sources in VTI media. (*a*) Records of *Vx* component; (*b*) records of *Vy* component; (*c*) records of *Vz* component.

phase is coincident. Though the amplitudes are different, their decay modes seem alike between them. As is known, Green's function is the analytic solution while the numerical solution of EWE is approximate. So there are some differences. However, the result is reliable (Coutant *et al* 1995).

As shown above, we can draw a conclusion that the new method is feasible and credible. SMT is an expression of source mechanisms and EWE can adapt to different media, whether homogenous or complex. Additionally, the SMT and EWE method can be used in combination to simulate the wave field and records with variety of sources.

3. Simulation and analysis

3.1. Simulation

To demonstrate the effectiveness of the SMT and EWE formulation, seismic responses for three basic kinds of sources (equations (7)–(9)) in four kinds of media are modeled. Table 1 shows the parameters of sources and their beachballs. The parameters of three sources: dip, slip and strike are shown which illustrate the faults in three dimensions.

There are 20 receivers in total from 240 to 560 m in depth. Each type of the source is located at (400, 400, 400 m). After the orientation correction of horizontal-components, the angles between microseismic events and receivers are very small on the horizontal plane. Thus, we set receivers with an angle of 0° in this direction. The vertical distance between source and receiver is 200 m.

Stiffness coefficients in four media are listed in table 2. We choose four representational media in this paper. For simplicity, the underground media can be assumed as homogeneous media or vertical transverse isotropy (VTI) media in a small area of microseismic monitoring. Most microseismic location methods use time lag based on this assumption. Here, we mainly discuss two kinds of media. With respect to the

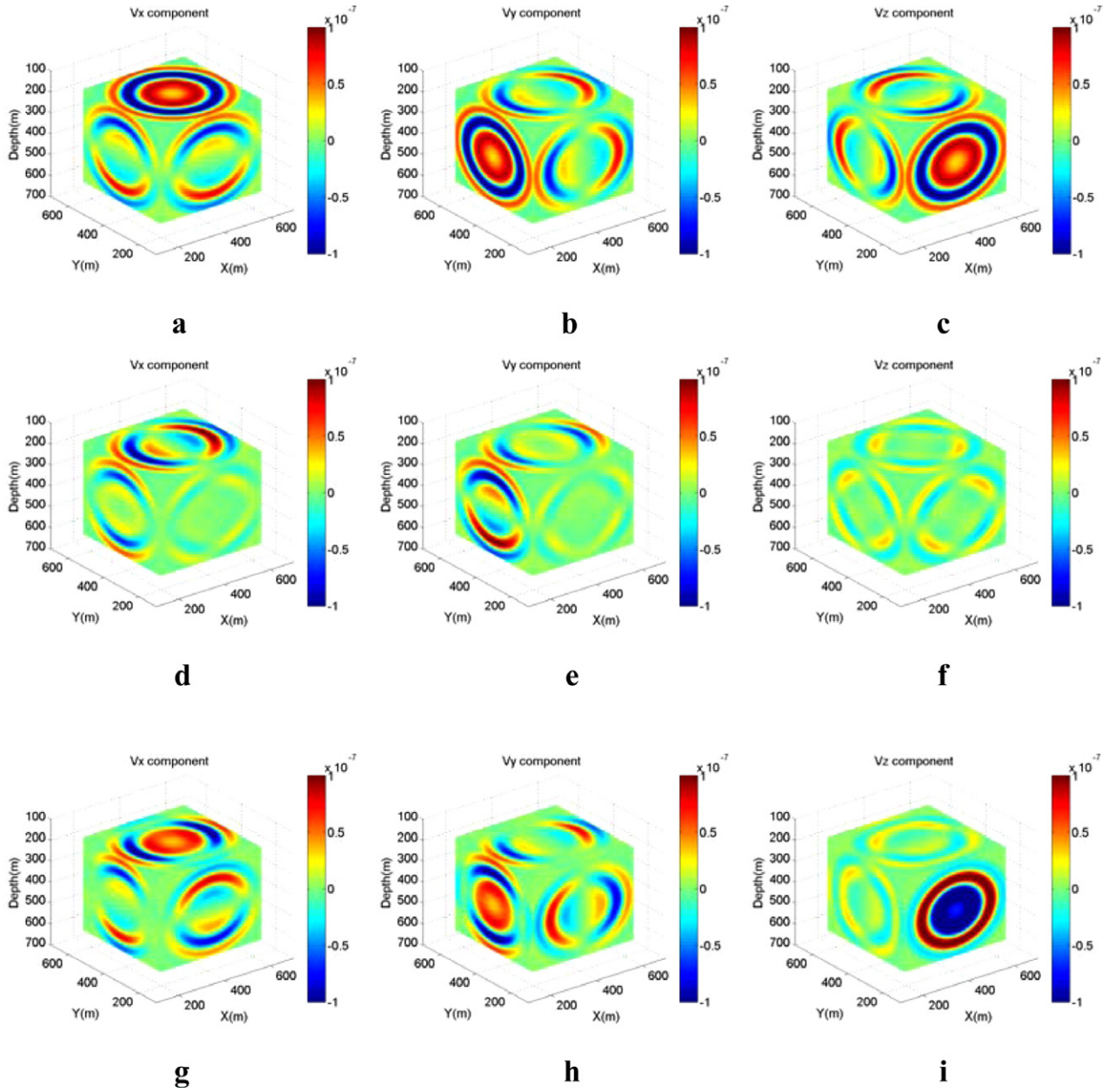

Figure 6. 3D wave fields of three components with three basic sources in homogeneous media. (*a*)–(*c*) are the 3D wave fields with ISO source; (*d*)–(*f*) are the 3D wave fields with DC source; (*g*)–(*h*) are the 3D fields with CLVD source.

calculations, we used staggered-grid FD method in the time-domain with a 800 × 800 × 800 m model. The grid size is 4 × 4 × 4 m. Time interval is 0.25 ms. The center frequency of the Ricker wavelet is 30 Hz.

Figure 4 shows the 3D three-component (3C) records of three kinds of sources in homogeneous media. From the modeling data, it can be seen that the amplitude of the P-wave in *Vx*, *Vz* components are stronger than *Vy* in ISO source simulation and a polarity reversal is observed in the *Vz* component. Meanwhile, in the case of the DC source, the energy of the S-wave in the *Vy* component is stronger than other two components. It can be regarded as a main energy wave. The records of CLVD are relatively complicated. As a result of the CLVD source occurring with the ISO source, the main characteristics of the wavefield in 3C acts in concert with ISO source. But the distinction is that the energy of the S-wave is stronger than the P-wave especially in *Vx* components and the S-wave does not appear in ISO source simulation. In the modeling of VTI media, the records maintain characteristics with homogeneous media apart from shear wave splitting. Fast and slow shear waves can be observed in three kinds of source simulations.

Figures 6–9 are the 3D three-component wave fields with three basic sources in four media at 75 ms. By comparing and analyzing 3D wave fields, we obtain the following results.

(a) ISO source: the wave fields in four different media sustain the basic characters of polarization. The difference among media is that the P-wave can only be obtained in homogenous media. The S-wave is much stronger than the P-wave in VTI media. This can also be observed in horizontal transverse isotropy (HTI) and orthotropic media.

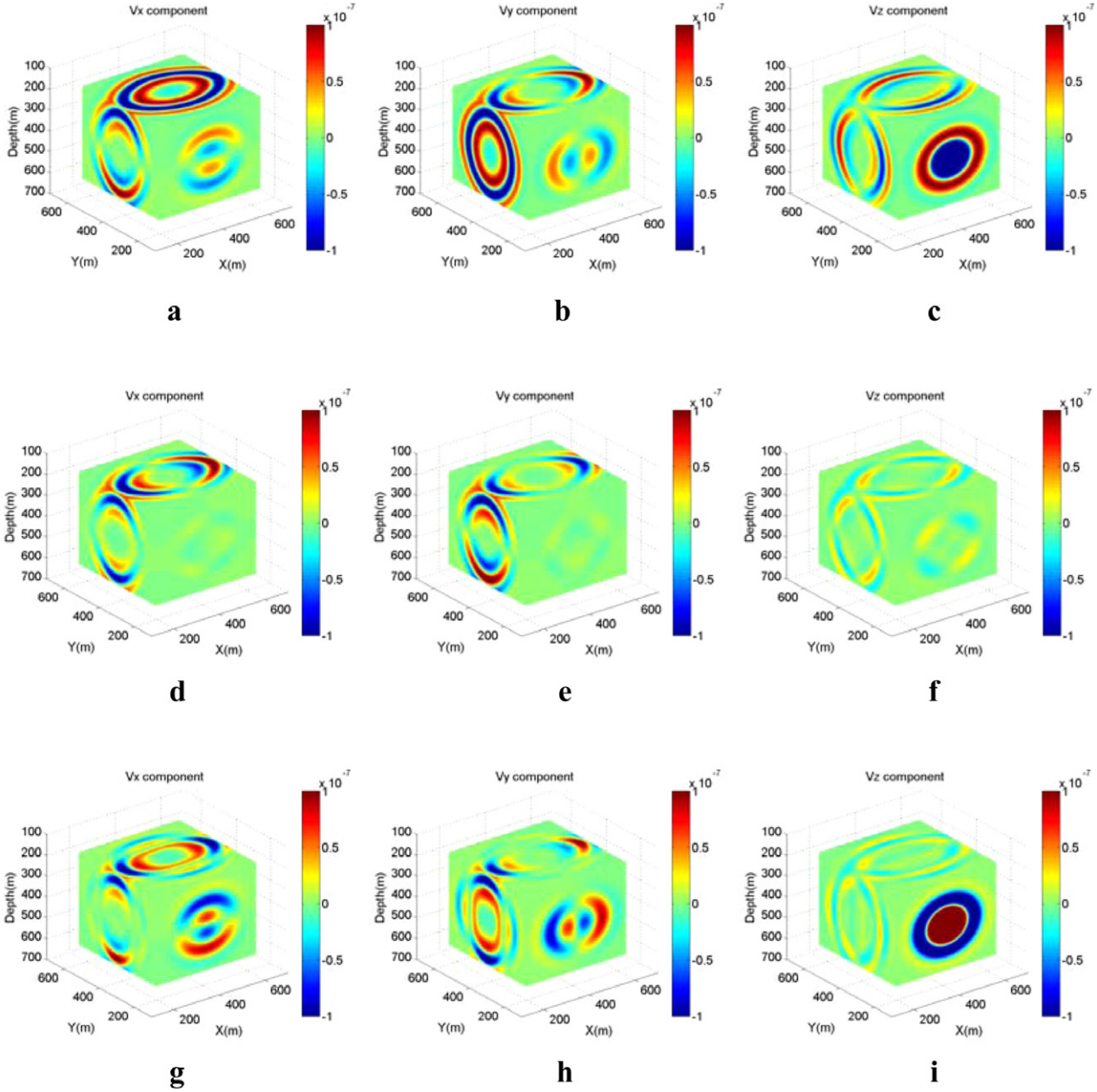

Figure 7. 3D wave fields of three components with three basic sources in VTI media. (*a*)–(*c*) are the 3D wave fields with ISO source; (*d*)–(*f*) are the 3D wave fields with DC source; (*g*)–(*h*) are the 3D fields with CLVD source.

(b) DC source: in homogenous, VTI and orthotropic media, the polarization features are consistent. But in the YOZ plane of the *Vx* component and XOY, YOZ planes of *Vz* components in HTI media are different from the other three media. This shows that the DC source is sensitive to HTI media.

(c) CLVD source: in contrast, the polarization characteristic shows no difference among four media except for the energy distribution.

3.2. Analysis

The polarization method has been applied in seismic exploration for many years (Gal'perin 1984). Previous studies using polarization features for filtering and wave field separation (Benhama *et al* 1988, Igor *et al* 1997, Richwalski *et al* 2001, Roueffa *et al* 2009, Lin *et al* 2014). In order to intensively study the polarization features with different sources in multiple media, we have analyzed the relationship between polarization angles and incidence angle.

Take a time window from three components data on the microseismic records, which include the P-wave. Assuming that, the array (x_i, z_i) is the value of the P-wave in the *Vx* and *Vz* components, where i is the sample number, the P-wave energy expression is shown as:

$$E(\theta) = \sum_i (x_i \cos\theta + z_i \sin\theta)^2 , \qquad (10)$$

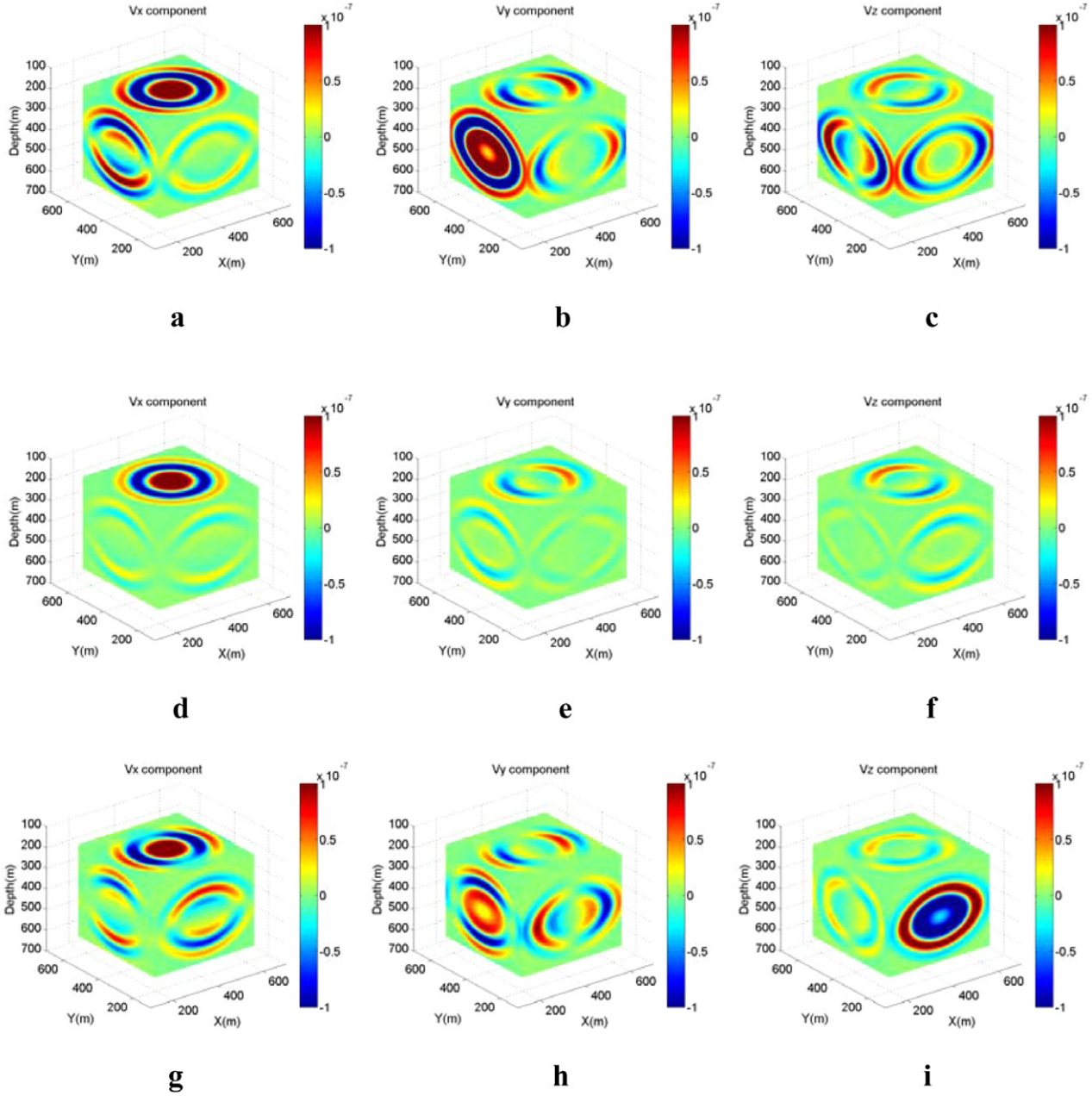

Figure 8. 3D wave fields of three components with three basic sources in HTI media. (*a*)–(*c*) are the 3D wave fields with ISO source; (*d*)–(*f*) are the 3D wave fields with DC source; (*g*)–(*h*) are the 3D fields with CLVD source.

where E is the energy, and θ is the rotation angle between the Vx and Vz components. When the value of E is maximum, it requires that

$$\frac{\partial E(\theta)}{\partial \theta} = 0, \tag{11}$$

so,

$$\sin(2\theta) \cdot \sum_i \left(z_i^2 - x_i^2\right) + 2\cos(2\theta) \cdot \sum_i x_i z_i = 0 \tag{12}$$

then

$$\tan(2\theta_{\max}) = \frac{2\sum_i x_i z_i}{\sum_i \left(x_i^2 - z_i^2\right)}, \tag{13}$$

where $\theta_{\max}$ is the polarization angle between the Vx and Vz components. We realize that the polarizing angle of the Vx and Vz components is relative with incident angle. That is to say, polarization direction changes with offset.

Figure 10 shows the curves of the three sources in four different media. In the same media, the curves of the ISO source and DC source are similar. Their polarization angles decrease as the incidence angles increase. But there is a sudden change at 30–50° of incidence angle in CLVD source simulations. For different media (figure 11), curves of the same sources are different. We can easily distinguish the VTI and HTI curves, while homogeneous and orthotropic curves are between them. Especially in the graph of the CLVD source, the differences are obviously in different media. The sudden change appears around the range of 35–50° in homogenous media, 25–35° in

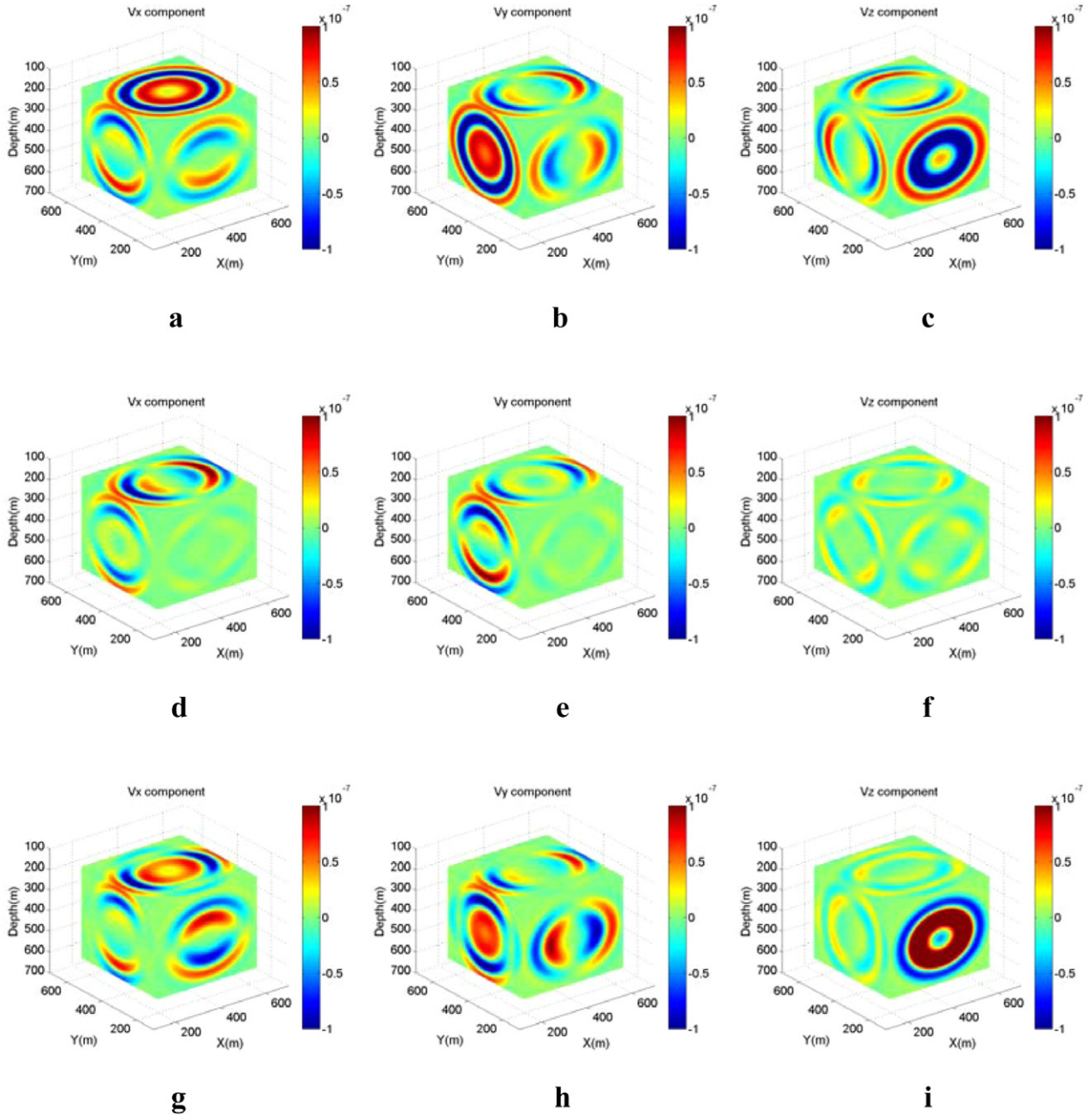

Figure 9. 3D wave fields of three components with three basic sources in orthotropic media. (*a*)–(*c*) are the 3D wave fields with ISO source; (*d*)–(*f*) are the 3D wave fields with DC source; (*g*)–(*h*) are the 3D fields with CLVD source.

VTI media, 40–55° in HTI media and 35–45° in orthotropic media. So, we can use this feature to distinguish VTI and HTI media.

4. Conclusions

The source mechanism in microseismic monitoring is complicated and diversified. Predecessors use seismic moment tensor to simplify this problem into three basic sources: ISO, DC and CLVD. This paper outlines basic sources excitation method used SMT and EWE based on the staggered-grid finite-difference approach. Expressions were given for the distribution of body force in three components, and it was pointed out how to generate ISO, DC and CLVD sources by finite-difference schemes in a velocity field. We use the source excitation method simulating different kinds of sources in different media and draw the following conclusions.

(a) In ISO source simulations: the P-wave can be recorded in the *Vx* and *Vz* components in homogenous media without the S-wave. In other words, the energy of ISO source comes from the P-wave. The S-wave could be generated by the P-wave in anisotropic media.
(b) In DC source simulations: the energy mainly focuses on shear wave in the *Vy* component. The P-wave is caused by shear force in anisotropic media. DC source occurs in shear fault. This coincides with the simulation result.

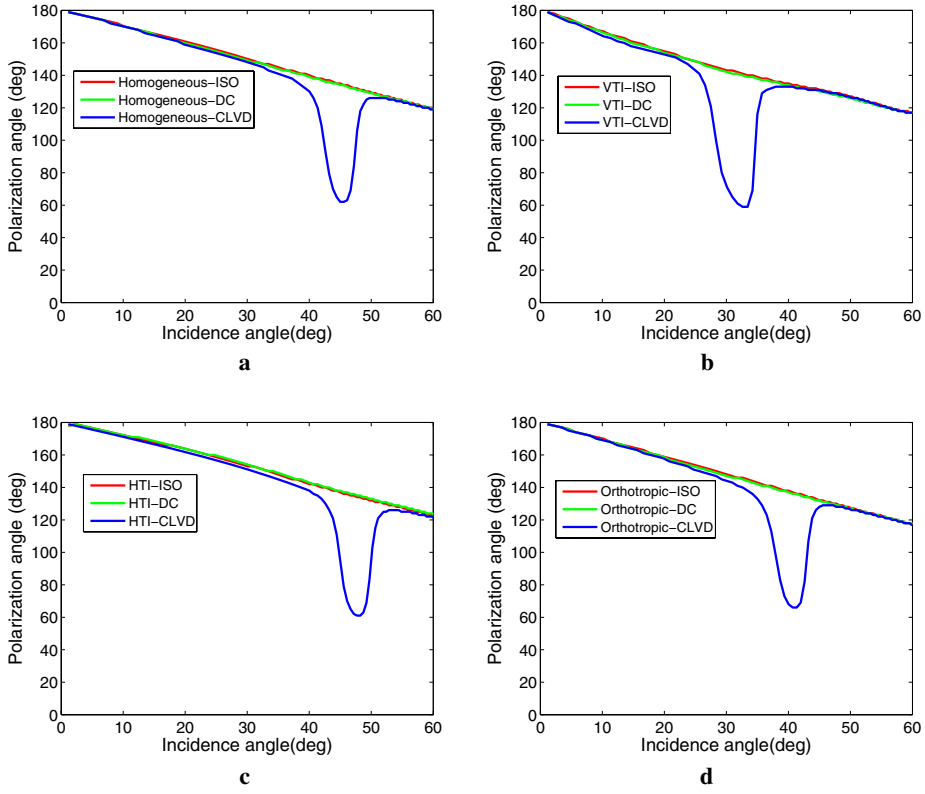

Figure 10. Relation between polarization angle and incidence angle with different sources in the same media. (*a*) Curves with three kinds of sources in homogenous media; (*b*) curves with three kinds of sources in VTI media; (*c*) curves with three kinds of sources in HTI media; (*d*) curves with three kinds of sources in orthotropic media.

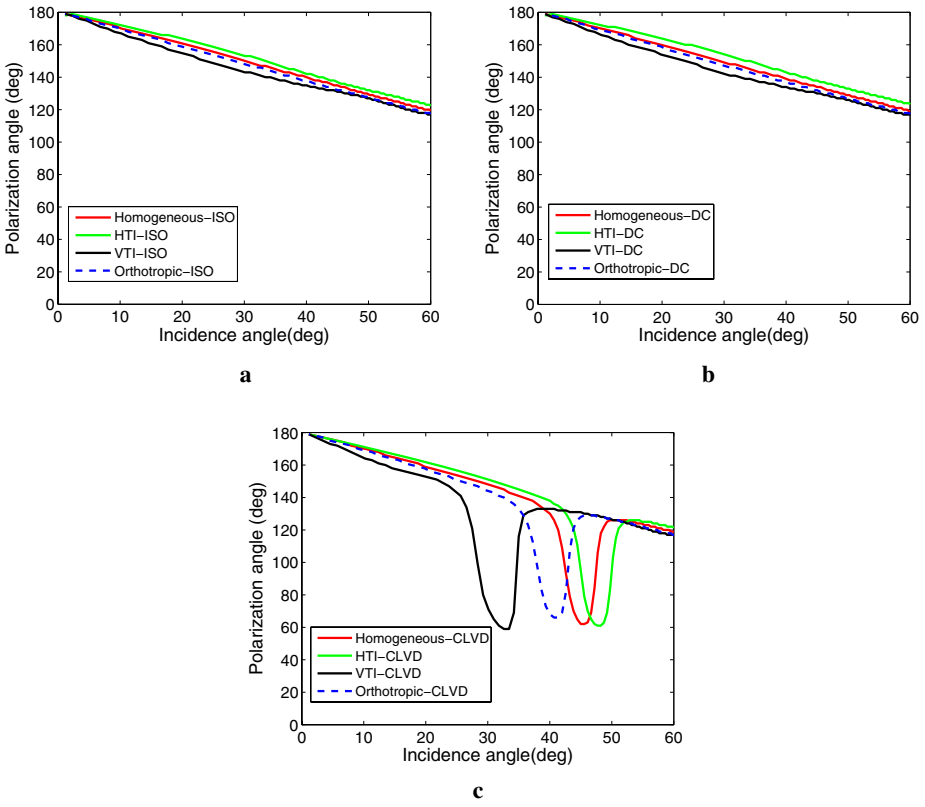

Figure 11. Relations between polarization angle and incidence angle with same sources in different media. (*a*) Curves with ISO source in different media; (*b*) curves with DC source in different media; (*c*) curves with CLVD source in different media.

(c) In CLVD source simulations: considering that the CLVD source couples with an ISO source, it should include some features similar to an ISO source which was verified in the records (figure 4(*c*)). On account of the non-uniform stress of CLVD source, an S-wave is generated and stronger than a P-wave (figures 4(*c*) and 5(*c*)).

(d) From the wave fields in different media, we can draw a conclusion that the DC source involved in this paper is sensitive to HTI media in figures 8(*d*)–(*f*). The reason is that the shear force of DC source lies on the XOY plane (figure 2), which could be parallel or perpendicular with HTI media.

(e) In the analysis of the polarizing angle and incident angle from the *Vx* and *Vz* components, the sudden change of curve is at 40–55° in HTI media and 25–35° in VTI media in figure 11(*c*). This would be an obvious way to distinguish HTI and VTI media. In homogeneous and orthotropic media, it is between them.

The DC and CLVD sources in this paper are just special cases which could also present other results. However, all of them are composed of the basic nine couple of force (Aki and Richards 2002). By using the expressions of nine couple of forces, we can simulate any kind of sources with SMT.

Acknowledgments

We are grateful to Sanyi Yuan, Chao Ma, Zhiming Ren and Xiaohui Cai for their constructive comments on this paper. Thanks to the anonymous reviewers for suggestions and comments which significantly improved our paper. We also would like to thank State Key Laboratory of Petroleum Resources and Prospecting for the computation platform. This research was supported by national major project (2011ZX051019-008-02) and CNPC major fundamental research program (2011A-3605)

Appendix

In the source excitation method, expressions for the distribution of the body force components *fy* and *fz* are similar with the equations discussed above in the text for the *fx* component. These expressions are

$$fy_{i,j+1/2,k} = \frac{M_{21}\cdot \mathrm{d}t}{\rho\cdot V\cdot \mathrm{d}x}\cdot f(t)\,, fy_{i-1,j+1/2,k} = -\frac{M_{21}\cdot \mathrm{d}t}{\rho\cdot V\cdot \mathrm{d}x}\cdot f(t)\,, \quad \text{(A1)}$$

$$fy_{i,j+1/2,k} = \frac{M_{22}\cdot \mathrm{d}t}{\rho\cdot V\cdot \mathrm{d}y}\cdot f(t)\,, fy_{i,j-1/2,k} = -\frac{M_{22}\cdot \mathrm{d}t}{\rho\cdot V\cdot \mathrm{d}y}\cdot f(t)\,, \quad \text{(A2)}$$

$$fy_{i,j+1/2,k} = \frac{M_{23}\cdot \mathrm{d}t}{\rho\cdot V\cdot \mathrm{d}z}\cdot f(t)\,, fy_{i,j+1/2,k-1} = -\frac{M_{23}\cdot \mathrm{d}t}{\rho\cdot V\cdot \mathrm{d}z}\cdot f(t)\,, \quad \text{(A3)}$$

$$fz_{i,j,k+1/2} = \frac{M_{31}\cdot \mathrm{d}t}{\rho\cdot V\cdot dx}\cdot f(t)\,, fz_{i-1,j,k+1/2} = -\frac{M_{31}\cdot \mathrm{d}t}{\rho\cdot V\cdot \mathrm{d}x}\cdot f(t)\,, \quad \text{(A4)}$$

$$fz_{i,j,k+1/2} = \frac{M_{32}\cdot \mathrm{d}t}{\rho\cdot V\cdot \mathrm{d}y}\cdot f(t)\,, fz_{i,j-1,k+1/2} = -\frac{M_{32}\cdot \mathrm{d}t}{\rho\cdot V\cdot \mathrm{d}y}\cdot f(t)\,, \quad \text{(A5)}$$

$$fz_{i,j,k+1/2} = \frac{M_{33}\cdot \mathrm{d}t}{\rho\cdot V\cdot \mathrm{d}z}\cdot f(t)\,, fz_{i,j,k-1/2} = -\frac{M_{33}\cdot \mathrm{d}t}{\rho\cdot V\cdot \mathrm{d}z}\cdot f(t)\,. \quad \text{(A6)}$$

References

Aki K and Richards P G 2002 *Quantitative Seismology* 2nd edn (Herndon, VA: University Science Books) pp 37–59

Baig A and Urbancic T 2010 Microseismic moment tensors: a path to understanding frac growth *Leading Edge* **29** 320–24

Bansal R and Sen M K 2008 Finite-difference modelling of S-wave splitting in anisotropic media *Geophys. Prospect.* **56** 293–312

Benhama A, Cliet C and Dubesset M 1988 Study and application of spatial directional filtering in three-component recordings *Geophys. Prospect.* **36** 591–613

Červený V 2001 *Seismic Ray Theory* (Cambridge: Cambridge University Press)

Coutant O, Virieux J and Zollo A 1995 Numerical source implementation in a 2D finite difference scheme for wave propagation *Bull. Seismol. Soc. Am.* **85** 1507–12

Gal'perin E I 1984 *The Polarization Method of Seismic Exploration* (Dordrecht: Reidel)

Graves R W 1996 Simulating seismic wave propagation in 3D elastic media using staggered-grid finite differences *Bull. Seismol. Soc. Am.* **86** 1091–106

Holfold R L 1981 Elementary source-type solutions of the reduced wave equation *J. Acoust. Soc. Am.* **70** 1427–36

Igor B M, Carr B J and Smithson S B 1997 P- and SV-wave separation by polarization-dependent velocity filtering: application to vertical seismic profiles from Kola superdeep borehole, Russia *Comput. Geosci.* **23** 1051–61

Jeng S K and Liu C H 1987 Wave propagation in media with three-dimensional quadratic refractive index profile *J. Acoust. Soc. Am.* **81** 1732–40

Knopoff L and Randall M J 1970 The compensated linear-vector dipole: a possible mechanism for deep earthquakes *J. Geophys. Res.* **75** 4957–63

Li YL, Liu C H and Franke S J 1990 3D Green's function for wave propagation in a linearly inhomogeneous media—the exact analytic solution *J. Acoust. Soc. Am.* **87** 2285–91

Lin F *et al* 2014 Polarization of plane wave propagating inside elastic hexagonal system solids *Phys. Mech. Astron.* **57** 251–62

Maxwell S 2010 Microseismic: growth born from success *Leading Edge* **29** 338–43

Olsen K B, Archuleta R J and Matarese J R 1995 Magnitude 7.75 earthquake on the San Andreas fault: three-dimensional ground motion in Los Angeles *Science* **270** 1628–32

Richwalski S, Roy-Chowdhury K and Mondt J C 2001 Multi-component wavefield separation applied to high-resolution surface seismic data *J. Appl. Geophys.* **46** 101–14

Roueffa A, Rouxd P and Réfrégier P 2009 Wave separation in ambient seismic noise using intrinsic coherence and polarization filtering *Signal Process.* **89** 410–21

Tsvankin I 2012 *Seismic Signatures and Analysis of Reflection Data in Anisotropic Media* 3rd edn (Tulsa, OK: Society of Exploration Geophysicists) pp 1–10

Vavryčuk V 2000 Acoustic and elastodynamic 3D Green's functions for isotropic media with a weak velocity gradient *Wave Motion* **31** 223–36

Vavryčuk V 2001 Inversion for parameters of tensile earthquakes *J. Geophys. Res.* **106** 16339–55

Vavryčuk V 2005 Focal mechanisms in anisotropic media *Geophys. J. Int.* **161** 334–46

Yomogida K and Etgen J T 1993 3D wave propagation in the Los Angeles Basin for the Whittier-Narrows earthquake *Bull. Seism. Soc. Am.* **83** 1325–44

Yuan S Y, Wang S X, Sun W J, Miao L N and Li Z H 2014 Perfectly matched layer on curvilinear grid for the second-order seismic acoustic wave equation *Explor. Geophys.* **45** 94–104